PAPER

Experimental investigation of sheath effects on I-V traces of strongly electron emitting probes

To cite this article: Chi-Shung Yip et al 2020 Plasma Sources Sci. Technol. 29 025025

View the article online for updates and enhancements.



IOP ebooks™

Bringing together innovative digital publishing with leading authors from the global scientific community.

Start exploring the collection-download the first chapter of every title for free.

Plasma Sources Sci. Technol. 29 (2020) 025025 (10pp)

https://doi.org/10.1088/1361-6595/ab60dd

Experimental investigation of sheath effects on *I–V* traces of strongly electron emitting probes

Chi-Shung Yip¹, Chenyao Jin¹, Wei Zhang^{1,3}, Guo Sheng Xu^{1,3} and Noah Hershkowitz²

E-mail: zhangwei@ipp.ac.cn and gsxu@ipp.ac.cn

Received 24 April 2019, revised 7 November 2019 Accepted for publication 11 December 2019 Published 24 February 2020



Abstract

I–V traces of strongly emitting emissive probes are investigated in a multidiople filament discharge. It is found that at sufficiently high neutral pressure and emitting current, the variation of the *I–V* traces and their associated inflection points no longer follow the previous predictions of space charge limited (SCL) models. A new, steep slope region of the *I–V* trace appears near the plasma potential when the probe is strongly emitting, causing the inflection point and the floating potential to increase towards the plasma potential as emission current increases, rather than staying constant. This is, to our knowledge, the first experimental evidence that the effects predicted by Campanell *et al*'s inverse sheath theory (2017 *Physics of Plasmas* **24** 057101) not only affect the floating potential but also a region in the *I–V* trace of an emissive probe. It is also found that the double inflection point structure when the probe is biased below the ionization energy of the working gas is highly likely to be an emission retardation effect from enhanced virtual cathode formation due to the increased local electron density. The implications of these findings on hot cathode sources are briefly discussed.

Keywords: sheaths, plasma diagnostics, electron emission, basic plasma physics

Introduction

Emissive probes are common diagnostics in the experimental studies of basic plasma physics- [1], thruster- [2, 3] and fusion-related research [4]. Emissive probes are especially important in diagnosing the plasma potential, as Langmuir probes generally fail to distinguish between global electron drift and potential changes [5]. Emissive probes can also be used as a direct measurement of sheath thickness through observing the reversal of the slope of the inflection voltage $V_{\rm inf}$ versus the emission current $I_{\rm emit}$ due to the reversal of electron- emission-affected space-charge effects in the plasma bulk and in the sheath [5, 6]. Work has also been done on the automation of emissive probes for use in measuring plasma and vacuum potential [7, 8].

Previous theoretical and experimental works state that virtual cathodes cause strongly electron emitting probes to float at approximately two times the electron temperature $2kT_{\rm e}/e$ below the plasma potential [5, 9]. More importantly, these works showed that if the emission current increases, the inflection point decreases first nonlinearly, then roughly linearly, and then finally becomes constant and independent of the emission current.

Recent studies [10-13] argue that inverse sheaths, instead of virtual cathodes, form near strongly emitting surfaces, allowing them to float above the plasma potential. Indeed, previous studies showed that strongly emitting probes can float higher than the plasma potential measured by cold probes [14]. However, it is known that I-V traces of the cold probes do not distinguish between electron drift and plasma potential changes. In addition, it is also of interest whether and to what extent inverse sheath formation would remain the dominant mechanism in sheath formation near the probe beyond the floating potential, which in turn decides the characteristics of the I-V trace.

0963-0252/20/025025+10\$33.00 1 © 2020 IOP Publishing Ltd

¹ Institute of Plasma Physics, Chinese Academy of Sciences, Hefei 230031, People's Republic of China ² Department of Engineering Physics, University of Wisconsin—Madison, Madison, Wisconsin 53706, United States of America

³ Authors to whom any correspondence should be addressed.

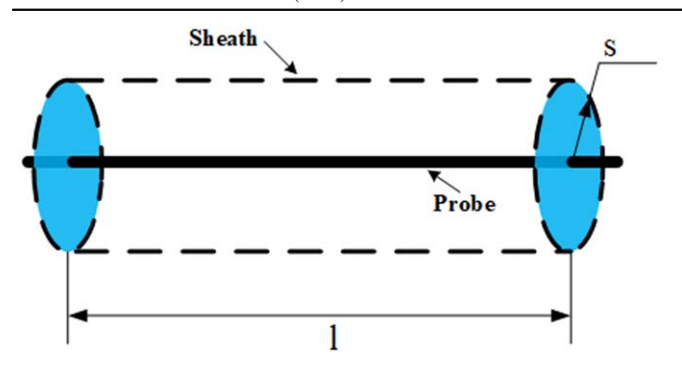


Figure 1. Geometry schematic of the probe's sheath structure.

Sheath formation and the resultant I–V characteristics of an emitting surface are also of interest for understanding hot cathode electron sources since they are, by nature, electron emitting surfaces. Sheath formation limits their emission current, which ultimately limits the performance and the parameter range within which they can operate [15]. It should also be noted that the kinetic energy of electrons injected into the plasma by the cathode sources is determined by the sheath potential drop. Therefore, the sheath effects of these strongly emitting surfaces also limits whether these sources can be used to heat [16] or cool [17] the plasma electrons. This study presents experimental results on how effects associated with very strong emission (the emission current $I_{\rm emit}$ being greater than 50–100 times the probe's electron saturation current $I_{\rm es}$) affect an emissive probe's entire I–V trace.

Virtual cathode near an emissive probe

Whether a virtual cathode or an inverse sheath forms is a question of whether the accumulated net negative charge in the virtual cathode is neutralized by ions trapped in the virtual cathode. To understand this effect, consider the emissive probe as an electron emitting cylindrical electrode, as shown in figure 1. The probe's sheath thickness s and the probe's length l_{probe} form a cylindrical volume around the probe. As electron emission from the probe increases, a virtual cathode forms if the probe bias is close to the plasma potential, due to the accumulation of electrons. Meanwhile, ions trapped within the virtual cathode can fill up the potential dip resulting in it being reduced [18] or, if completely filled up, the formation of an inverse sheath [12].

In the absence of ion trappings, the thickness of the virtual cathode s can be calculated solving Poisson's equation assuming Maxwellian plasma electrons with temperature $T_{\rm e}$, emitted electrons with temperature $T_{\rm te}$, and mono-energetic ions:

$$\frac{d^2\chi}{d\xi^2} = \frac{n_{\text{te,xmin}}}{n_{\text{e,s}}} \exp\left(\frac{T_{\text{e}}}{T_{\text{te}}}\chi\right) \left(1 \pm \operatorname{erf}\left(\sqrt{\frac{T_{\text{e}}}{T_{\text{te}}}}\chi\right)\right) \\
+ \exp(\chi - \chi_s) - \frac{n_{\text{i,s}}}{n_{\text{e,s}}} \left[1 - \frac{2(\chi - \chi_s)}{M^2}\right]^{-\frac{1}{2}}$$
(1)

with the boundary conditions derived employing the Sagdeev potential approach used by Wang *et al* [19, 20]. Here $n_{\text{te,xmin}}$ is

the emitted electron density voltage minimum point x_{\min} of the virtual cathode, $n_{\rm e,s}$ and $n_{\rm i,s}$ are the plasma electron and ion density at the sheath edge, $\chi \equiv e(\varphi - \varphi_m)/T_{\rm e}$ where φ is the local potential, $\xi \equiv x/\lambda_{\rm Debye}$ is the Debye length, $\lambda_{\rm Debye}$ the normalized length, and M is the Mach number v_i/c_s . The plasma electrons are assumed to satisfy the Boltzmann relation:

$$n_{\rm e} = n_{\rm es} \exp\left[\frac{e(\Phi - \Phi_{\rm s})}{T_{\rm e}}\right] \tag{2}$$

where T_e is the electron temperature, φ is the local potential and φ_s is the potential at the sheath-presheath boundary $\chi = \chi_s$. With ion-collisions neglected, the ion density is determined by flux and energy conservations:

$$\frac{1}{2}m_i v_i^2 + e\Phi = \frac{1}{2}m_i v_{is}^2 + e\Phi_s \tag{3}$$

$$n_i v_i = n_{is} v_{is} \tag{4}$$

where v_i and v_{is} are the ion velocity at χ and χ_s respectively, and n_{is} is the ion density at the sheath edge. The ion density can be written:

$$n_i = n_{is} \left[1 - \frac{2e(\Phi - \Phi_s)}{m_i v_{is}^2}\right]^{-\frac{1}{2}}.$$
 (5)

For emitted electrons with temperature T_{te} , the spatial density of these electrons is then given by:

$$n_{\text{te}\pm} = n_{\text{te}0} \exp\left[\frac{e(\Phi - \Phi_0)}{T_{\text{te}}}\right] \left[1 \pm \text{erf}\left(\sqrt{\frac{e(\Phi - \Phi_m)}{T_{\text{te}}}}\right)\right]$$
(6)

where the plus and minus signs denote the region between the surface of the electrode and the bottom of the virtual cathode, and that from the bottom of the virtual cathode to the bulk plasma. n_{te0} is the density of the emitted electrons at the emitting electrode. φ_0 and φ_m are the potentials at the emitting electrode and the bottom of the virtual cathode and erf(x) is the error function.

Taking $T_{\rm e} \approx 1.5\,{\rm eV},~T_{\rm te} \approx 0.2\,{\rm eV},~{\rm and}~n_{\rm e} = 4\times 10^9\,{\rm cm}^{-3},$ the resultant potential structure is numerically solved and shown in figure 2 at different emission current $I_{\rm emit}$ normalized by the electron collection current $I_{\rm es}$. As shown in the figure, the virtual cathode approximately spans 10 Debye lengths, which is approximately 1.5 mm. Decreasing the plasma density or increasing the electron temperature increases the Debye length. With $s \propto \lambda_{\rm Debye}$, one can approximate the change in s by the change in $\lambda_{\rm Debye}$. For our experimental parameters, the Debye length ranges from 0.15 mm to 0.6 mm as shown in table 1, which accounts for an approximate range of the size of the virtual cathode from 1.5 mm to 6 mm.

As ions fall into the sheath and travel through the virtual cathode, charge exchange occurs and ions with zero-velocity are produced from the background neutral gas to replace moving ions. Zero-velocity ions are also produced from the high energy tail of the electron energy distribution function as

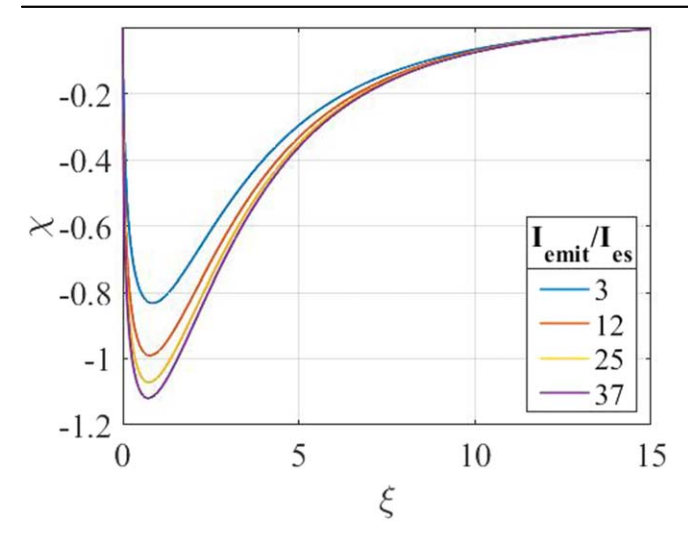


Figure 2. Virtual cathode potential structure computationally resolved using Wang *et al*'s method [19] at different emission current, assuming no ion filling.

well as from primary electrons. The production rates of ions per volume are given by:

$$Z_{j-n} = \Gamma_j n_n \sigma_{j-n} \tag{7}$$

where n_n is the neutral density, σ_{j-n} is the collisional cross section between particle j and the neutral gas, and v_i is the velocity with which particle species *i* enter the sheath. $\Gamma_i = n_i v_i$ is the per unit area flux of ions or electrons streaming through that volume. High-energy electrons, coming from the tail of the bulk electron energy distribution function (EEDF) or primary electrons, stream through the sheath volume being marginally affected by the virtual cathode potential, as the electron energy required for ionization processes (>15.7 eV) is much higher than any possible energy loss in the virtual cathode (<1 eV). Thus the volume production rate is $(\pi s^2 l) n_n \int n_{e,b} f(E) \sigma_{e,b-n}(E) (2E/m)^{1/2} dE$ for ionization from the tail of the Maxwellian and approximately $(\pi s^2 1) \sum_k n_{\text{pri},k} v_k n_n \sigma_{k-n}$ for the primaries, where k is the number of times ionization collisions take place before the primaries are thermalized into the tail of the bulk Maxwellian EEDF. For primary electron energy $E_{\rm pri} > 60 \, {\rm eV}$, the effects of multiple ionizations per primary electron must be considered and the exact bulk EEDF must be considered in order to calculate the ionization contribution from its high energy tail. For the ion-neutral charge exchange rate, the per unit area flux of ions $\Gamma_i = (s/r)n_iv_i$ into the virtual cathode depends on the position where collisions occur due to the cylindrical geometry, i.e. $n_i = n_0(v_{i0}/v_i)(s/r)$, where r is the radial position and n_0 is the bulk plasma density. To account for zero-velocity ion production over the whole virtual cathode we integrate Z_{i-n} from the radius of the probe to the radius of the sheath, resulting in the volume production rate $n_i = (2\pi s^2 l) n_0 v_{i0} n_n \sigma_{i-n} (\ln(s/r_{\text{probe}}))$ where r_{probe} is the probe radius. Here $n_n \sigma_{i-n} = 1/\lambda_{i-n}$ is the ion-neutral collision mean free path. Using $\sigma_{i-n} \approx 10^{-14}$ cm² [21], the corresponding λ_{i-n} variation in our experiment is approximately 1 cm to 41 cm corresponding to a neutral pressure range of 0.01 Pa to 0.4 Pa. In addition, ions orbiting around the probe can be trapped radially within the virtual cathode. These ions fill up the virtual cathode and increase the charge exchange production of zero-velocity ions. We also presented in table 1 the variation of the ionization mean free path of the energetic primary electrons with different neutral pressure and primary energy $E_{\rm pri}=60\,{\rm eV}$. However, the comparison of this mean free path with the other lengths is not intuitive as the electron density relevant to this collision is the primary density $n_{\rm pri}$, not the plasma density $n_{\rm e}$ or the emitted electron density $n_{\rm te}$. The density of the primary energetic electrons of a multidipole confined filament discharge is determined by both the discharge current and the loss area for the primary electrons, which is reduced from the geometric chamber wall area by the multi-dipole confinement.

Zero-velocity ions created within the virtual cathode are radially trapped within the structure because they do not have sufficient kinetic energy to escape. In the absence of other effects, any ion production results in virtual cathode filling, if the ions cannot escape the virtual cathode. However, experimentally ions can always be pumped away because emissive probes have dielectric supporting structures which allow ions to escape [18]. With an emissive probe, this loss area exists at the two ends of the probe. Thus, the trapped ion loss rate can be approximated as:

$$L_{i,VC} = A_{loss} n_{i,VC} v_{i,VC}$$
 (8)

where $n_{\rm i,VC}$ and $v_{\rm i,VC}$ are the density and axial escape velocity of the trapped ions, and $A_{\rm loss}$ is the area to which these ions are lost. This is the cylindrical area covered by the virtual cathode πs^2 when the end cross-section of the cylindrical volume is covered by the sheaths of the dielectric supports, or can be the area of the dielectric supports (or its sheath) when s is large. One should note that this ion loss is different from bulk plasma ion loss to a sheath as the virtual cathode itself is a sheath structure, thus $v_{\rm i,VC}$ is not necessarily $c_s = (T_{\rm e}/m_i)^{1/2}$, the Bohm velocity.

One can see that the πs^2 term in the total ion production and total ion loss mechanisms approximately cancel each other out, but an expansion of the virtual cathode sheath length s may stretch out its volume, resulting in a reduced trapped ion density. Table 1 lists the experimental neutral pressures and their associated plasma parameters in this work. One can see that the Debye length (associated with the sheath length s) is changed by approximately 4.6 times within this work's parameter range, and the ion–neutral collision length changed by 40 times. The ionization rate is expected to have a similar change as the primary electron energy and discharge current are unchanged, which results in the production rate being mostly affected by the neutral pressure.

An extreme example of this virtual cathode filling, by one mechanism or another, is when the virtual cathode is completely filled up and the net electron emission is limited purely by the probe's bias voltage. The *I–V* trace will thus saturate at temperature-limited emission once the probe is biased below the plasma potential and the net emission current reduces only when the probe is biased above the plasma potential, when the probe itself forms an electron sheath to repel the emitted electron back to the probe. Then under

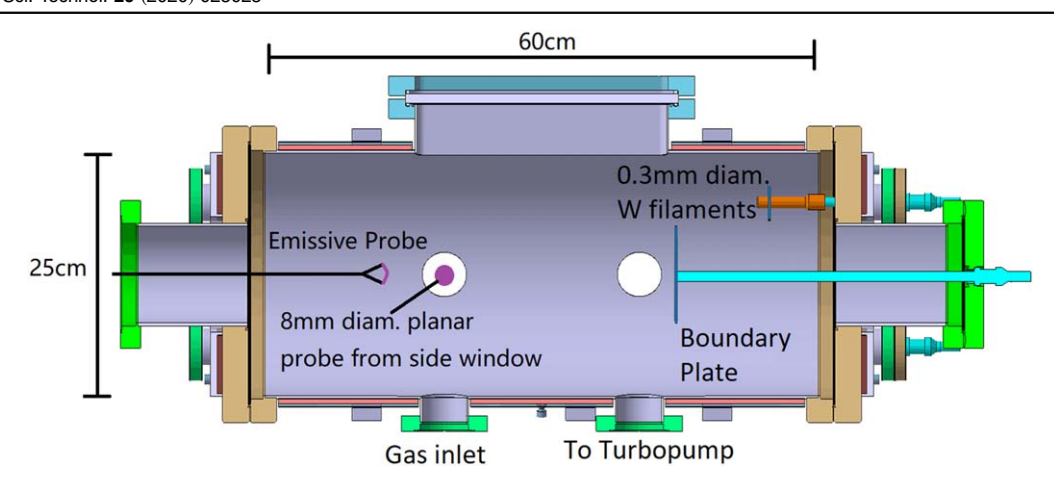


Figure 3. A schematic of the multi-dipole chamber.

Table 1. Experimental parameters in this work. For all neutral pressures the discharge current is 0.5 A.

Neutral Pressure (Pa)	$T_{\rm e}~({\rm eV})$	$n_{\rm e} \ (\times 10^9 {\rm cm}^{-3})$	Debye length (mm)	λ_{i-n} (cm)	$\lambda_{\text{pri-}n}$ (cm)
0.4	1.34 ± 0.07	$3.84 \pm 0.2 \times 10^9$	0.14 ± 0.01	1	39
0.2	1.56 ± 0.1	$4.00 \pm 0.2 \times 10^9$	0.15 ± 0.01	2	77
0.1	1.66 ± 0.1	$3.40 \pm 0.17 \times 10^9$	0.16 ± 0.01	4.1	155
0.07	1.93 ± 0.15	$2.60 \pm 0.13 \times 10^9$	0.2 ± 0.015	5.9	221
0.04	2.36 ± 0.25	$1.56 \pm 0.1 \times 10^9$	0.29 ± 0.015	10	387
0.01	3.75 ± 0.3	$5\pm0.25\times10^8$	0.645 ± 0.015	41	1547

strong emission, both the emission current's inflection point and the floating potential will be higher than the plasma potential, with the floating potential, for example, being [22]:

$$\ln\left(\frac{I_{\text{emit}}}{I_{\text{es}}}\right) = \frac{e(V_{\text{f}} - V_{\text{p}})}{T_{\text{te}}} - \frac{1}{2}\ln\left(1 + \frac{e(V_{\text{f}} - V_{\text{p}})}{T_{\text{te}}}\right). \quad (9)$$

A noteworthy effect in the formation of virtual cathodes is that secondary electron emission on the surface of the probe is potentially close to unity [23–25]. This results in a deeper virtual cathode as the electrons are bounced multiple times between the bottom of the virtual cathode and the probe surface, increasing the local electron density and thus the depth of the virtual cathode. This increases the number of ions required to fill up the virtual cathode.

A precise computational study of this loss-production balance within the emissive probe's virtual cathode requires precise knowledge of the sheath structure and is best studied with a 3D simulation; it is thus out of the scope of this work.

Experimental setup

Experiments were performed in a multi-dipole confined [26] filament discharge via the impact ionization of energetic (primary) electrons, shown in figure 3. The device consists of a 25 cm diameter, 60 cm long vacuum chamber. Primary electrons are produced by a set of two 0.3 mm diameter, 10 cm long tungsten filaments near the end wall opposite to the boundary plate to provide a discharge current $I_{\text{Dis}} = 0.5 \text{ A}$ at a bias of -60 V. Sixteen rows of permanent magnets

surround the radial wall, creating a multi-dipole confinement to trap ionizing energetic electrons and produce a uniform plasma. The device's dimension is thus not the relevant length for energetic electrons to be lost before ionizing a neutral as they can bounce multiple times within the multi-dipole surface confinement. Note that with multi-dipole confinement, the magnetic field lines are connected to the surface of the magnets, resulting in a magnetic field rapidly reducing and becoming approximately zero (or the Earth's magnetic field) at the center of the device, resulting in an unmagnetized plasma. An additional 12 rows of magnets are also positioned on each side of the end walls to create a cusp, reducing axial electron loss. A 10 cm diameter boundary plate made of stainless steel is inserted through one end of the chamber. The boundary plate is kept floating for this study. The base vacuum of the chamber is at 5×10^{-4} Pa and operated at 0.01-0.4 Pa argon neutral pressure. One should note that with a filament discharge, the EEDFs contain Maxwellian electrons and primary electrons. The primary electrons are the main source of ionization [27, 28] and the tail of the Maxwellian provides little contribution to plasma production. Therefore, Maxwellian EEDFs are maintained even at very low degrees of ionization. An I-V trace in a 0.4 Pa argon plasma showing an EEDF without a depleted tail is shown in figure 4.

Langmuir probes and emissive probes are inserted through the axial and radial walls to perform measurements of the electron temperature $T_{\rm e}$, the plasma density $n_{\rm e}$, and the local potential $V_{\rm p}$. The windows where these probes are inserted into the chamber are indicated in figure 1. The

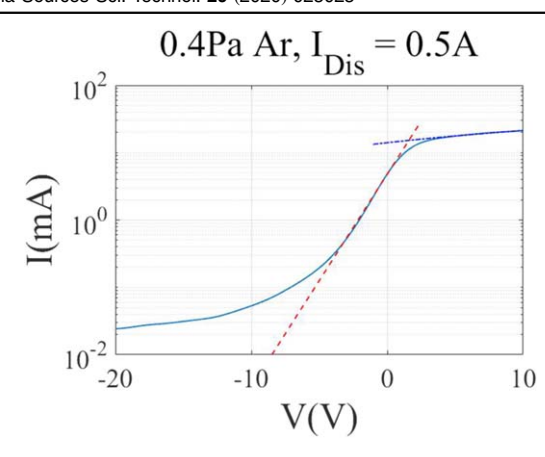


Figure 4. A Langmuir probe I-V trace taken in the 0.4 Pa argon plasma.

movable range of the emissive probe spans from the boundary plate to 20 cm away from it, and that of the planar Langmuir probe spans the diameter of the chamber. Emissive probe data in this experiment are taken 10 cm away from the boundary plate.

The schematics of the Langmuir and emissive probe tip assemblies are presented in figure 5. Here, 0.01 mm and 0.12 mm diameter tungsten wires are used as emissive probe tips. These tips are connected through 0.3 mm diameter copper tubes or copper-plated stainless-steel wires running through 1.5 mm diameter double-holed ceramic tubes to connect into the wire leads in the 4 mm diameter stainless steel probe shaft. At the probe tips the copper tubes form a Y-shape, covered by 0.8 mm diameter single-holed ceramic tubes, giving the emissive probes a 6-7 mm span. The Langmuir probes consist of an 8 mm diameter plate spot welded onto 0.8 mm diameter copper-plated stainless-steel wires, covered by 2 mm diameter single-holed ceramic tubes to connect to the 4 mm diameter stainless steel probe shaft. A schematic of the emissive probe's sweeping and heating circuitry is illustrated in figure 6. Probe emission current in this study ranges from $I_{\text{emit}} = 0$ to $I_{\text{emit}} > 0.1$ A. One should note that the maximum emission current from the probe is comparable to the discharge current (0.5 A), which may result in increased electron density, but only when the probe's bias is very negative. In this study we are interested in two regions of the probe's *I–V* trace: near the plasma potential, where most of this additional current is still confined by the probe's electron sheath and does not produce additional plasma through ionization; and when the probe is biased below at least the ionization energy below the plasma potential, where the additional ionization, as discussed in the next section, explains the effects observed in this work.

Results and discussion

Figure 7 shows a family of I-V traces taken with the 0.12 mm diameter emissive probe in a plasma 10 cm from the bias plate in a 0.4 Pa argon neutral pressure plasma. Previous studies [5, 9] of emissive probe I-V traces show that the trace of an

emitting probe can be divided into three regions: a collecting region, a space charge limited region (SCL) and a temperature-limited region (TL). These traces consist of only one inflection point unless the ionization effect is present [29], and the inflection point progressively decreases as emission increases, then eventually becomes constant. The temperature-limited emission region where emission saturates, and the collection region where sheath expansion limits the probe's current can be observed at the right and left extremes of figure 7. However, with very strong emission ($I_{\text{emit}} > 25$ $I_{\rm es}$), a new region appears near the plasma potential where the slope of the I-V trace becomes much steeper, and then the slope flattens again once biased a few volts below the plasma potential; this region is labelled 'Inverse?' in figure 7. This continues until another knee-like feature appears and the emission current converges to a second, larger saturation current. This is better illustrated in the dI/dV versus V graph in figure 8, where the inflection point near the plasma potential begins to split with increasing emission current. The new, steep region of the I-V trace near the plasma potential causes the highest inflection point to move towards the plasma potential as the emission current increases, and another, smaller inflection point emerges which continues to become more negative. As shown in figures 7 and 8, at low emission the three-stage I-V trace can be retrieved, and at high emission, the inflection point which progressively becomes more negative also seems to agree with previous studies [5, 9]. However, these previous studies did not show the new, steep slope region near the plasma potential which results in the new inflection point increasing towards the plasma potential as emission increases. Virtual cathodes are known to reduce emission current [5, 6, 9], resulting in flattened *I–V* traces with decreasing inflection points. The reverse of this effect suggests that the depth of the virtual cathode has been reduced, resulting in an increased net emission when the probe is biased near the plasma potential, thus with a steeper slope of the *I–V* trace. This increase of net emission is a phenomenon indicated in more recent studies associated with the inverse sheath formation [10, 12, 14].

In figure 9, the inflection points V_{inf} and the floating potential of the I-V traces shown in figures 7 and 8 are graphed. Conventionally, a straight line is fit to the $V_{\rm inf}$ versus I_{emit} graph and the plasma potential is determined by extrapolating the line to zero emission. This is known as the inflection point technique in the limit of zero emission and has been shown to be an accurate measurement of the plasma potential as long as the maximum I_{emit} is of the same order of magnitude as the electron saturation current I_{es} [3]. This is illustrated in figure 9(a) using the inflection points below $I_{\rm es} = 1.6 \pm 0.1$ mA. At a greater emission current, a new phenomenon is observed. As shown in figure 9(b), the inflection points reach a minimum at approximately $I_{\rm emit}=10\,I_{\rm es}$, and then increases again as emission increases, approaching the plasma potential. This is different from previous predictions which state that the inflection point will be independent of the emission current once a minimum is reached, as emission current increases. In addition, the floating potential $V_{\rm f}$, where the probe's total current is zero,

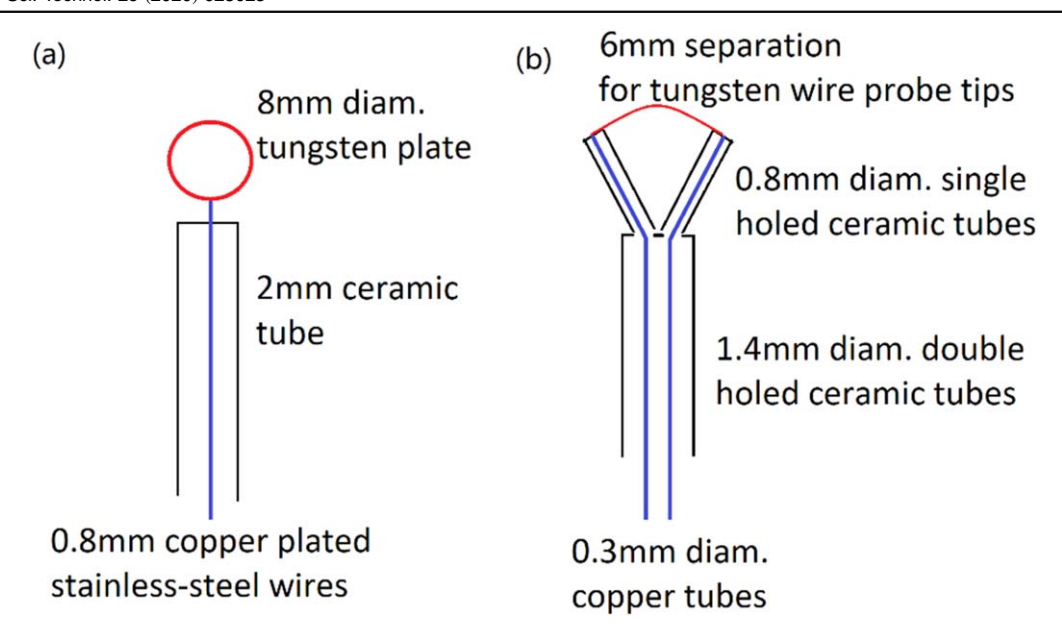


Figure 5. Schematics of the Langmuir probe (a) and the emissive probe (b).

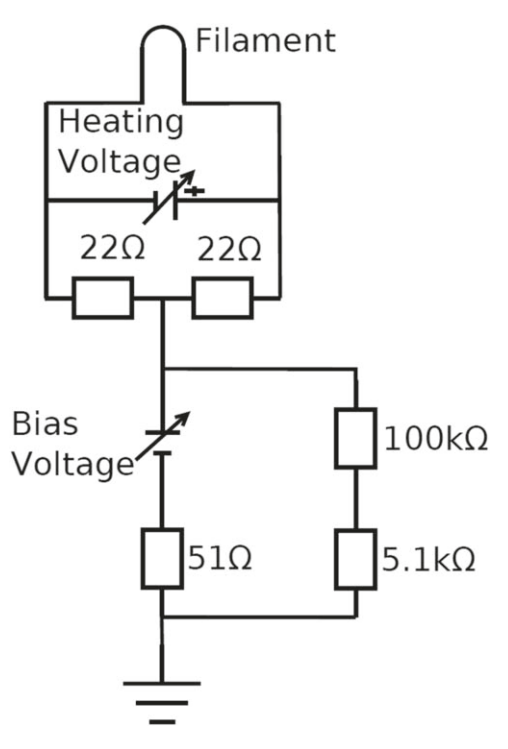


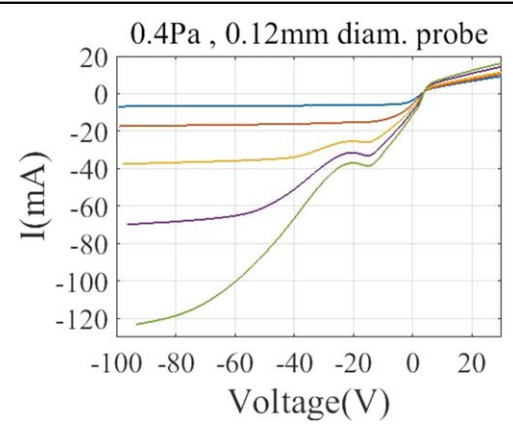
Figure 6. Circuit diagram of the emissive probe.

increases with the emitting current and eventually exceeds the plasma potential as measured by the inflection point technique when $I_{\rm emit} > 35~I_{\rm es}$, above which the increase in the floating potential seems to saturate with increasing emission. This also means that at a very high emission current the floating point technique might result in a measured plasma potential higher than the potential measured by the inflection point technique in the limit of zero emission, in contrast to previous results [2]. Again, previous studies show that inflection points become more negative and eventually become constant as emission increases while virtual cathodes limit the net

emission current [5, 9]. The observation that the inflection points trend back towards the plasma potential as emission increases means a higher portion of the emitted current leaves the virtual cathode to the bulk plasma at a higher probe voltage, the same effect corresponding to the slope of the I-Vtrace being steepened in figure 7. This suggests that the depth of the virtual cathodes and their emission limiting effect has been reduced. This result shows that with sufficient emission, virtual cathode formation alone is inadequate in determining the sheath structure of the strongly emitting probe when biased near the plasma potential, and that ion filling effects, associated with inverse sheath formation, start to become significant [10]. It is important to note that although the inflection points increase with emission current, they were never higher than the plasma potential as measured by the inflection point technique. Therefore, this shows that the virtual cathode has been reduced, and not filled up, as discussed in the previous section.

If ion-neutral collisionality, as indicated by Campenall *et al*, determines whether a virtual cathode or inverse sheath can be observed, then lowering the neutral pressure should reproduce *I–V* traces and their associated inflection points similar to previous results [5, 9]. Indeed, the case of the three-stage feature found in previous studies [5, 9] can be retrieved for all probes if the neutral pressure is sufficiently low.

This is shown in figure 10, which graphs a series of emission current versus inflection point trends for two different emissive probes in a series of different neutral pressures. As shown in the figure, the three-region model from Ye's SCL description can only describe the I-V trace and inflection point variation for low neutral pressure cases, and only for the 0.01 mm probe when the neutral pressure is sufficiently high. For the 0.12 mm diameter probe, the inflection point voltage increases towards the plasma potential once it reaches a minimum, as also shown in figure 10. However, if the neutral pressure is sufficiently lowered, or for



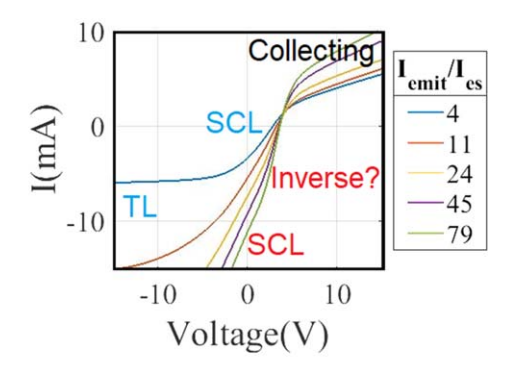


Figure 7. The 0.12 mm diameter emissive probe I-V traces (a), and these I-V traces magnified for the region near the plasma potential (b) of various temperature-limited emissions in a 0.4 Pa. The 'Inverse?' label indicates the new, steeper region in the I-V trace.

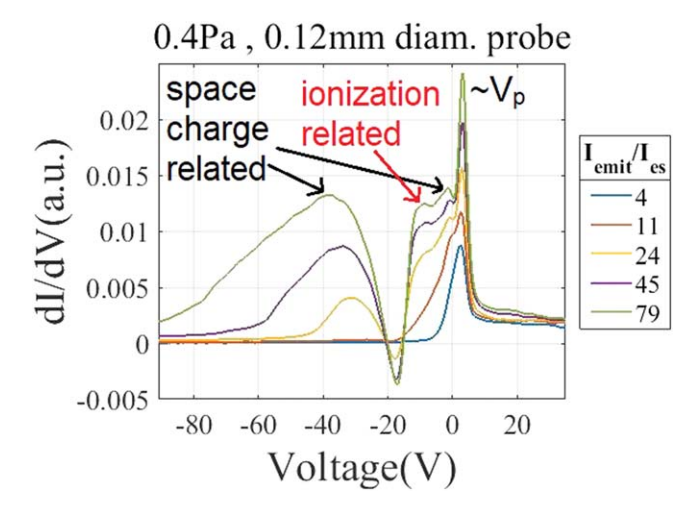


Figure 8. dI/dV of the I-V traces shown in figure 7.

a very small probe radius, the inflection point stays constant once it reaches a minimum, retrieving previous experimental and computational results exhibiting I-V traces dominated by SCL effects [3, 9].

With the change of the ion-neutral collision mean free path λ_{i-n} changing from 2 cm to 41 cm and the approximate length scale of the virtual cathode s changing from 1.5 mm to 6 mm in the parameter range shown in figure 7, λ_{i-n}/s changed from 13 to 68 in our experiment. The results show that as λ_{i-n}/s increases, the evolution of the inflection points as indicated by previous studies [5, 9] can be retrieved, indicating that effects associated with virtual cathodes determine the evolution of the inflection points. On the other hand, with decreasing λ_{i-n}/s , even at a ratio of approximately 33, one can see that the inflection points are starting to move towards the plasma potential, indicating that the virtual cathode filling effect is at work. This suggests that neutral collisionality is a deciding factor of whether the conventional space charge limited model can describe the variation of the inflection points, agreeing with recent studies [10, 12, 14].

One should remember that ion loss to the dielectric support limits the accumulation of ions within the virtual cathode, and is thus pivotal to the retrieval of the SCL dominated I–V characteristics. The experimental results also

show that even at higher neutral pressures, a smaller probe exhibits SCL dominated I-V traces at higher neutral pressures. This is because an emissive probe with a smaller radius generates a higher local emitted electron density due to a smaller adjacent volume, requiring more ions to fill up the virtual cathode, even when the emitted current is normalized by the probe's area. The I-V traces and their respective inflection points for the 0.01 mm diameter probe are graphed in figure 11, where it can be seen that the one-peak $\mathrm{d}I/\mathrm{d}V$ features, as seen in previous studies [5, 9], are successfully reproduced.

The observation of an additional feature near one ionization energy divided by electron charge $E_{\rm iz}/e$ is consistent with previous works, which argue that ionization effects increase the apparent emission current due to the extra ion current created by the local ionization of the energetic emitted electrons [29]. However, even if every single emitted electron creates an additional ion to be absorbed by the probe, the ionelectron square-rooted mass ratio $(m_i/m_e)^{1/2} \approx 271$ will result in a very small additional current. With argon ionization energy at 15.7 eV and the impact-ionization cross section only becoming significant at above 30 eV electron energy, as well as the short length scale of the sheath (a few mm) and the presheath (a few cm), ionization by emitted electrons within the sheath would be scant because the electron requires much of the energy from the sheath drop to impact ionize an atom, limiting these ionization effects near or out of the sheath boundary towards the bulk plasma. Thus, a significant additional current due to new ions collected by the probe is unlikely. Furthermore, if ionization increases the apparent emission current through the local creation of more ions to be absorbed by the probe, the removal of this effect by decreasing the neutral pressure should cause the emission current to saturate at the emission current where the I-V trace has apparently saturated before ionization effects increase the current into the probe again.

Instead, when we significantly lower the neutral pressure to 0.01 Pa and at a similar heating power to the probe, the second inflection point corresponding to the ionization effects fades, but the emission current increases almost linearly, and eventually becomes approximately the same as those of the I–V

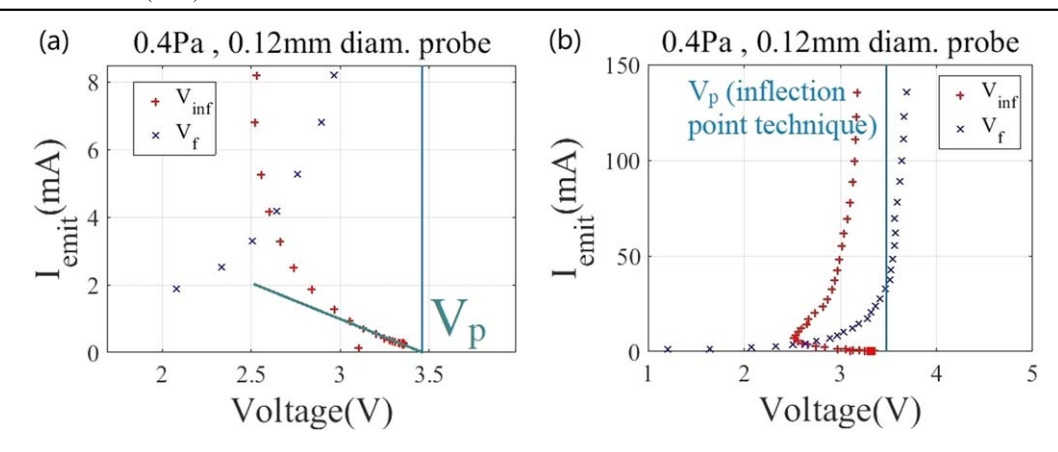


Figure 9. The inflection points $V_{\rm inf}$ and floating potential $V_{\rm f}$ of 0.12 diameter emissive probe $I\!-\!V$ traces in a 0.4 Pa, $I_{\rm Dis}=0.5$ A plasma. In this plasma the electron saturation current $I_{\rm es}=1.55\pm0.1$ mA. The blue vertical line is the plasma potential determined by the inflection point technique in the limit of zero emission.

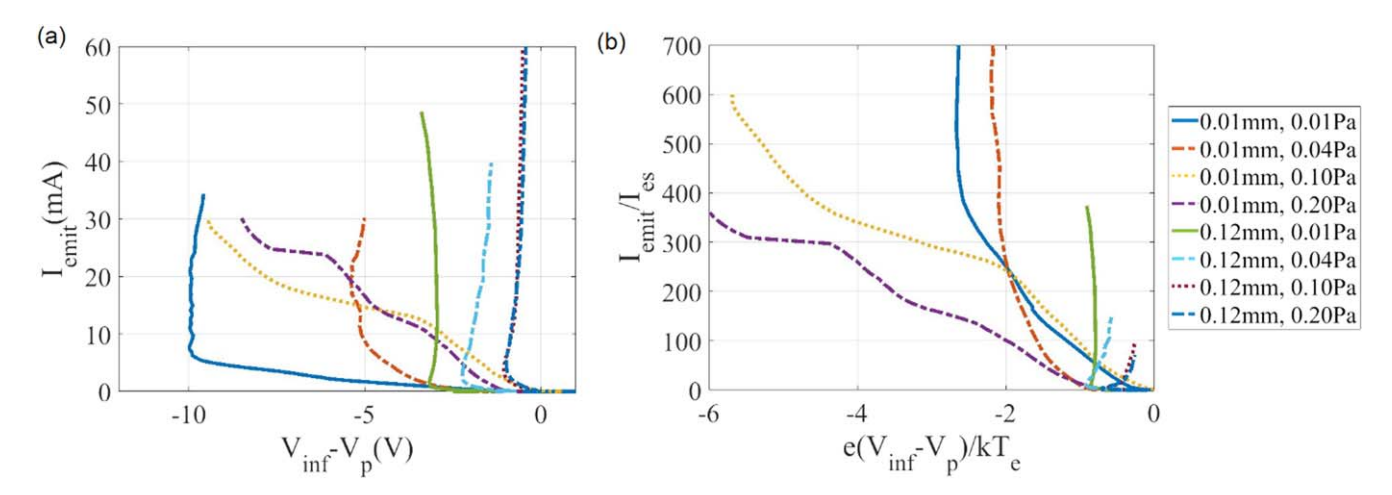


Figure 10. The inflection point versus emission current in different argon neutral pressure plasmas for 0.01 mm and 0.12 mm diameter emissive probes.

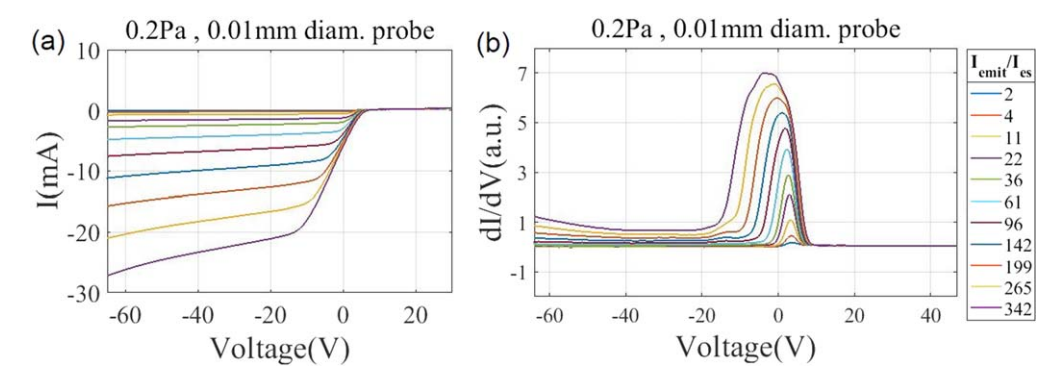


Figure 11. The I-V traces (a) and their respective inflection points in a 0.2 Pa neutral pressure, $I_{\rm Dis}=0.5$ A argon plasma.

traces taken in higher neutral pressures, as shown in figures 12(a) and (b). Shown in the figure are multiple I–V traces of the same emissive probe at a similar heating power. As shown in the figure, at similar heating power the maximum emission current at $-100 \, \text{V}$ is very similar, but traces taken at a higher neutral pressure saturate at a smaller negative bias to a temperature-limited current. Once we normalize the bias voltage by the electron temperature $kT_{\rm e}/e$, however, the I–V traces taken at higher neutral pressure emit less current when biased

beyond an ionization energy $E_{\rm iz}/e$ lower than the plasma potential, until they too saturate to a temperature-limited current at a lower $kT_{\rm e}/e$ normalized voltage. This suggests that the change in I–V traces associated with ionization effects were, in fact, sheath effects associated with virtual cathode formation. When the probe is strongly emitting and as the electron energy increases with the probe bias beyond the argon ionization energy of 15.7 eV, ionization begins near but outside of the probe's sheath (since electrons are likely to need most or all the

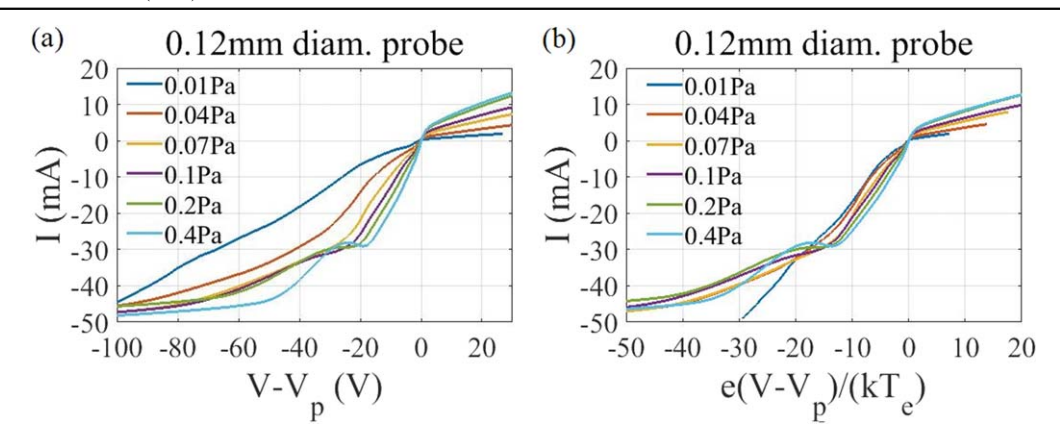


Figure 12. (a) I-V traces of the 0.12 diameter emissive probe at various neutral pressures at similar heating parameters. (b) T_e normalized I-V traces from the same experiments.

potential energy from the sheath to ionize neutral gases). This increases the local plasma density near the probe and causes the Debye length to shrink, which in turn causes the probe to become larger with respect to the Debye length and become more physically planar. A larger radius or more planar probe is known to cause a deeper virtual cathode to form near its surface, causing emission current to be suppressed, which in turn causes the *I*–*V* trace to flatten near the bias voltage in question. In fact, it can be observed in figure 7 that just E_{iz}/e below the plasma potential, the emission current is—for a short voltage range reduced rather than increased as the bias voltage decreases. This is further evidence that the ionization effect is not a current creating effect. This strongly suggests that, in contrast to previous understanding [29], ionization effects are in fact an emission retardation effect caused by enhanced virtual cathode formation rather than additional ion current into the probe.

Conclusion

The *I–V* characteristics of strongly emitting emissive probes are experimentally investigated. It is found that at moderate neutral pressure (>0.1 Pa argon) and very strong emission $(I_{\rm emit} > 50 I_{\rm es})$, the results of previous emissive sheath studies by Ye et al and Sheehan et al [5, 9] would fail to describe both the variation of the I-V trace and that of the inflection points as the emitted current increases. Experimental results suggest that the effects described by Campenall et al's study on inverse sheath formation [10–13, 30] can influence the I-Vcharacteristics of a strongly emitting probe in a voltage region near the plasma potential, causing the strongly emitting inflection point and the floating potential to increase beyond the conventionally predicted V_p - kT_e/e . To our knowledge, this is the first experimental evidence of inverse sheath effects not only affecting the floating potential but also a proportion of the I-V trace of an emissive probe. This suggests that electrons can be emitted at a very low energy from a cathode source so that the plasma is cooled [17] rather than heated by injecting thermionically emitted electrons.

It is also found that the effect previously described as added ion current due to ionization effects is highly likely to be an emission current suppression effect due to enhanced virtual cathode formation near the probe because of increased local electron density. This strongly suggests that if a hot cathode source is operating in such a voltage regime, any observed additional current is highly likely to be the thermionic emission current from the cathode itself, and the energy of the added electron emission will retain the same energy as other emitted electrons. It should be noted that if the added current was, as previous studies suggests, to be an ion current created through ionizations, the additional electrons created by the ionization process would possess much lower kinetic energy than that determined by the bias voltage of the cathode, because these electrons will be created at a location where the local potential has at least an ionization energy higher (and most likely much higher) than the cathode's bias voltage.

Acknowledgments

This work is supported by the Chinese Academy of Science Hundred Youth Talent Program start-up funding, the CAS Key Research Program of Frontier Sciences grant no. QYZDB-SSW-SLH001, the National Natural Science Foundation of China contract no. 11875285, 11575248 and 11505220, as well as the US National Science Foundation award no. 1804654.

ORCID iDs

Chi-Shung Yip https://orcid.org/0000-0003-4475-8000 Wei Zhang https://orcid.org/0000-0002-9854-8028

References

- [1] Yip C S and Hershkowitz N 2015 Effect of a virtual cathode on the I–V trace of a planar Langmuir probe *J. Phys. D* 48 395201
- [2] Sheehan J P et al 2011 A comparison of emissive probe techniques for electric potential measurements in a complex plasma Phys. Plasmas 18 073501

- [3] Sheehan J et al 2016 Recommended Practice for Use of Emissive Probes in Electric Propulsion Testing J. Propulsion and Power 33 1–24
- [4] Balan P et al 2003 Emissive probe measurements of plasma potential fluctuations in the edge plasma regions of tokamaks Rev. Sci. Instrum. 74 1583–7
- [5] Sheehan J P and Hershkowitz N 2011 Emissive probes *Plasma Sources Sci. Technol.* 20 063001
- [6] Wang X and Hershkowitz N 2006 Simple way to determine the edge of an electron-free sheath with an emissive probe *Rev.* Sci. Instrum. 77 043507
- [7] Jianquan L I et al 2018 Automatic emissive probe apparatus for accurate plasma and vacuum space potential measurements. Plasma Sci. Technol 20 24002
- [8] Li J.-q. et al 2016 Improved inflection point method of emissive probe for accurate measurement of plasma potential J. Vacuum Sci. Technol. A 34 061304
- [9] Ye M Y and Takamura S 2000 Effect of space-charge limited emission on measurements of plasma potential using emissive probes *Phys. Plasmas* 7 3457–63
- [10] Campanell M D, Khrabrov A V and Kaganovich I D 2012 Absence of Debye sheaths due to secondary electron emission *Phys. Rev. Lett.* 108 255001
- [11] Campanell M D 2015 Entire plasmas can be restructured when electrons are emitted from the boundaries *Phys. Plasmas* 22 040702
- [12] Campanell M D and Umansky M V 2017 Are two plasma equilibrium states possible when the emission coefficient exceeds unity? *Phys. Plasmas* 24 057101
- [13] Campanell M D 2018 Alternative model of space-chargelimited thermionic current flow through a plasma *Phys. Rev.* E 97 043207
- [14] Kraus B F and Raitses Y 2018 Floating potential of emitting surfaces in plasmas with respect to the space potential *Phys. Plasmas* 25 030701
- [15] Campanell M D and Umansky M V 2017 Improved understanding of the hot cathode current modes and mode transitions *Plasma Sources Sci. Technol.* 26 124002
- [16] Hershkowitz N and Leung K N 1975 Plasma electron heating by injection of low-energy electrons. Appl. Phys. Lett. 26 607–9

- [17] Campanell M D and Johnson G R 2019 Thermionic cooling of the target plasma to a sub-eV temperature *Phys. Rev. Lett.* 122 015003
- [18] Forest C and Hershkowitz N 1986 Steady-state ion pumping of a potential dip near an electron collecting anode. *J. Appl. Phys.* 60 1295–9
- [19] Wang D-Y, Xiu J and Zhang W-G 2009 Sheath structure of a hot-cathode in plasma Acta Phys. Sin. 58 8432–9
- [20] Li W et al 2012 Measurement of virtual cathode structures in a plasma sheath caused by secondary electrons *Phys. Plasmas* 19 030704
- [21] Lieberman M A and Lichtenberg A J 2005 Principles of Plasma Discharges and Materials Processing 2nd edn (Hoboken, NJ: Wiley-Interscience) pp 757
- [22] Hershkowitz N 1989 How Langmuir probes work *Plasma Diagnostics*. (Boston: Academic)
- [23] Cimino R et al 2015 Detailed investigation of the low energy secondary electron yield of technical Cu and its relevance for the LHC Phys. Rev. Spec. Top.-AB 18 10
- [24] Cazaux J 2012 Electron back-scattering coefficient below 5 keV: analytical expressions and surface-barrier effects J. Appl. Phys. 112 8
- [25] Schiesko L et al 2008 Experimental study and modeling of the electron-attracting sheath: the influence of secondary electron emission Phys. Plasmas 15 9
- [26] Limpaecher R and MacKenzie K R 1973 Magnetic multipole containment of large uniform collisionless quiescent plasmas Rev. Sci. Instrum. 44 726–31
- [27] Yip C-S et al 2013 Mackenzie's Demon with instabilities Plasma Sources Sci. Technol. 22 065002
- [28] Kim N-K et al 2015 How to determine the relative ion concentrations of multiple-ion-species plasmas generated in the multi-dipole filament source J. Phys. D: Appl. Phys. 48 225201
- [29] Picková I et al 2006 Measurements with the emissive probe in the cylindrical magnetron Czech. J. Phys. 56 B1002–8
- [30] Wang X et al 2016 Plasma potential in the sheaths of electronemitting surfaces in space Geophys. Res. Lett. 43 525–31